Parametric study of Pulsed Field Ablation with biphasic waveforms in an in vivo heart model: the role of frequency

Tomás García-Sánchez, *PhD*[1, †], Gerard Amorós-Figueras, *PhD*[2, †], Esther Jorge *PhD*[2], María C. Campos, *MD*[3], Elad Maor, *MD, PhD*[4], Jose M. Guerra *MD, PhD*[2, ‡] and Antoni Ivorra, *Prof, PhD*[1,5, ‡]

[1] Department of Information and Communication Technologies, Universitat Pompeu Fabra, Barcelona, Spain

[2] Department of Cardiology, Hospital de la Santa Creu i Sant Pau, Institut d'Investigació Biomèdica - Sant Pau, Universitat Autònoma de Barcelona, Barcelona, Spain

[3] Department of Pathology, Hospital de la Santa Creu i Sant Pau, Universitat Autònoma. Barcelona, Spain.

[4] Chaim Sheba Medical Center, Tel Hashomer, Israel; Sackler School of Medicine, Tel Aviv University, Tel Aviv, Israel.

[5] Serra Húnter Fellow Programme, Universitat Pompeu Fabra, Barcelona, Spain

† - Equal contribution

‡ - Shared lastauthorship

Short title: Parametric study of Pulsed Field Ablation in vivo

Corresponding author:

- Full name: Tomás García Sánchez
- e-mail: tomas.garcia@upf.edu
- Address:

  Department of Information and Communication Technologies,

  Universitat Pompeu Fabra.

  Roc Boronat 138. 080018, Barcelona, SPAIN.

Total word count (including Title Page, Abstract, Text, References, Tables and Figures Legends): 7247

Abstract

BACKGROUND:

Pulsed field ablation (PFA) is a novel non-thermal cardiac ablation technology based on irreversible electroporation. Unfortunately, the characteristics of the electric field waveforms used in clinical and experimental PFA are not typically reported. This study examines the effect of the frequency of biphasic waveforms and compares biphasic to monophasic waveforms.

METHODS:

A total of 29 Sprague-Dawley rats were treated with PFA using an epicardial monopolar electrode. Biphasic waveforms with three different frequencies, 90, 260 and 450 kHz (10 bursts of 100 μs duration at 500 V or 800 V) and monophasic waveforms (10 pulses of 100 μs duration at 500 V) were studied. Collateral neuromuscular stimulation and temperature increase in the point of application were directly measured. Lesion formation was assessed 3 weeks after treatment by histopathologic analysis. Computer simulations were used to estimate the electric field lethal threshold for each condition. A previous in vitro study was performed to draw a complete characterization of the studied dependencies.

RESULTS:

Morphometric analysis demonstrated a significant association between chronic lesion size and waveform characteristics. For the same voltage level, monophasic waveforms yielded the largest lesions compared to any of the biphasic protocols ($p<0.05$). Increasing PFA frequency was associated with reduced neuromuscular stimulation but also with reduced ablation efficacy. Maximum absolute temperature increase recorded along a complete treatment was 3 °C. Vascular structures inside the lesions were preserved for all conditions. Computer simulation-based analysis showed that waveform frequency had a graded effect on the lethal electric field threshold, with threshold of 600 V/cm for monophasic waveforms vs. 2000 V/cm for biphasic waveforms with a frequency of 450 kHz.

CONCLUSIONS:

Frequency is a major determinant of efficacy in biphasic PFA. Our results highlight the critical need of disclosing waveform characteristics when reporting the results of different PFA systems.

Nonstandard Abbreviations and Acronyms

EP Electroporation

IRE Irreversible electroporation

ELF Electric Field

PFA Pulsed Field Ablation

Clinical perspective

What is Known

- Pulsed Field Ablation (PFA) is an emerging non-thermal technology for cardiac ablation based on irreversible electroporation with potential advantages over other technologies.
- Unfortunately, one of the major parameters that determines the outcome of PFA, the waveform configuration used to apply the electric field to cardiac tissue, is not disclosed by the companies developing the technology.

What the Study Adds

- This study shows how PFA waveform characteristics impact its efficacy, specifically it shows that biphasic PFA exhibits a clear dependency on the frequency of the waveform: lesion dimensions decrease as the frequency increases.
- While we observed a clear dependency of collateral neuromuscular stimulation on waveform characteristics, no differences in the histological features of the lesions were observed between different conditions.
- This study also describes the actual electric field threshold values necessary for cardiac PFA in vivo and their dependence on the characteristics of the waveform used.

Introduction

The use of irreversible electroporation (IRE) as a non-thermal method for ablation of cardiac arrhythmias, also known as Pulsed Field Ablation (PFA), has rapidly moved from preclinical studies to clinical application in recent years[1–6]. The IRE concept relates to the cell death induced as a consequence of electroporation, which is the transient increase in cell membrane permeability upon the application of a short and intense electric field.

Despite the apparent good results of the initial use of the technique[7], many of the mechanisms that drive lesion formation and its impact on safety and efficacy remain unclear. One of the major parameters that determine the outcome of any IRE treatment is the waveform configuration used to apply the electric field to tissue[8–11]. The specific roles of the type of waveform (square monophasic, square biphasic, sinusoidal, etc.), the frequency, the duration of each individual application (either a single pulse/cycle or a burst of pulses/cycles), the total number of applications and the delay between applications are unknown. Moreover, the preclinical and clinical development of the technology has been mainly driven by companies which have kept confidential most of the used waveform specific characteristics. Only few preclinical studies reported the actual characteristics of the used waveforms[12–15], or studied the effects that any of these parameters had in the efficacy of the treatment[16–18].

The understanding of the effects that the different waveform parameters have in PFA results is critical to draw a comprehensive picture of the phenomenon. Additionally, it will improve its safety and efficacy and will allow a fair comparison between the different protocols already in use (electric field threshold values for different protocols, possibilities of titration, equivalent dose analysis between different platforms, etc.).

In this work we performed a parametric study to understand how the frequency of biphasic waveforms modulates the efficacy and other collateral effects during a PFA treatment in an in vivo animal model. A monopolar electrode setup mimicking a focal ablation catheter was used. An analogous in vitro study in cells was previously carried to understand the dependencies

obtained in a wide range of parameters and to stablish the limits of the parameters used in the subsequent in vivo experiments.

Methods

The data that support the findings of this study are available from the corresponding author upon reasonable request.

Electric field waveform configuration

This study used two types of waveform: monophasic square pulses and biphasic square bursts. Each individual monophasic square pulse had a duration of 100 µs, and each complete treatment consisted of 10 pulses applied with an interpulse period of 1 s (i.e 10 seconds total treatment duration). The biphasic burst consisted of a packet of consecutive biphasic pulses with a total 100 µs duration per burst (a biphasic pulse consists of a positive pulse followed by a negative pulse with zero delay between them). Similarly, each treatment consisted of 10 bursts applied with a interburst period of 1 s (10 seconds total treatment time)(see Fi.g 1a). Different internal frequencies of the periodic biphasic square waveforms were studied. In particular, for the in vivo experiments, the studied frequencies were 90 kHz, 260 kHz and 450 kHz.

The different biphasic square bursts were assayed at two voltage levels: 500 V and 800 V. Monophasic pulses were only assayed at 500 V because a pilot study with the same setup showed complete transmural lesions at this voltage level (data not shown). The voltages used were chosen to limit transmurality of the lesions, thus allowing to accurately measure lesions dimensions, specially depth. All the voltages reported in the manuscript are peak amplitudes (V_p) (see Fig. 1a for a schematic representation of the waveform configurations used).

For the in vitro study, non-cardiac cells were exposed in suspension in electroporation cuvettes. A wide range of electric field (ELF) magnitudes was assayed for each waveform configuration. Namely, the biphasic frequencies assayed were 150 kHz, 250 kHz and 450 kHz, monophasic pulses were also used. Refer to Supplemental Materials for a detailed description of the methods used in the vitro experiments.

In vivo exposure setup and equipment

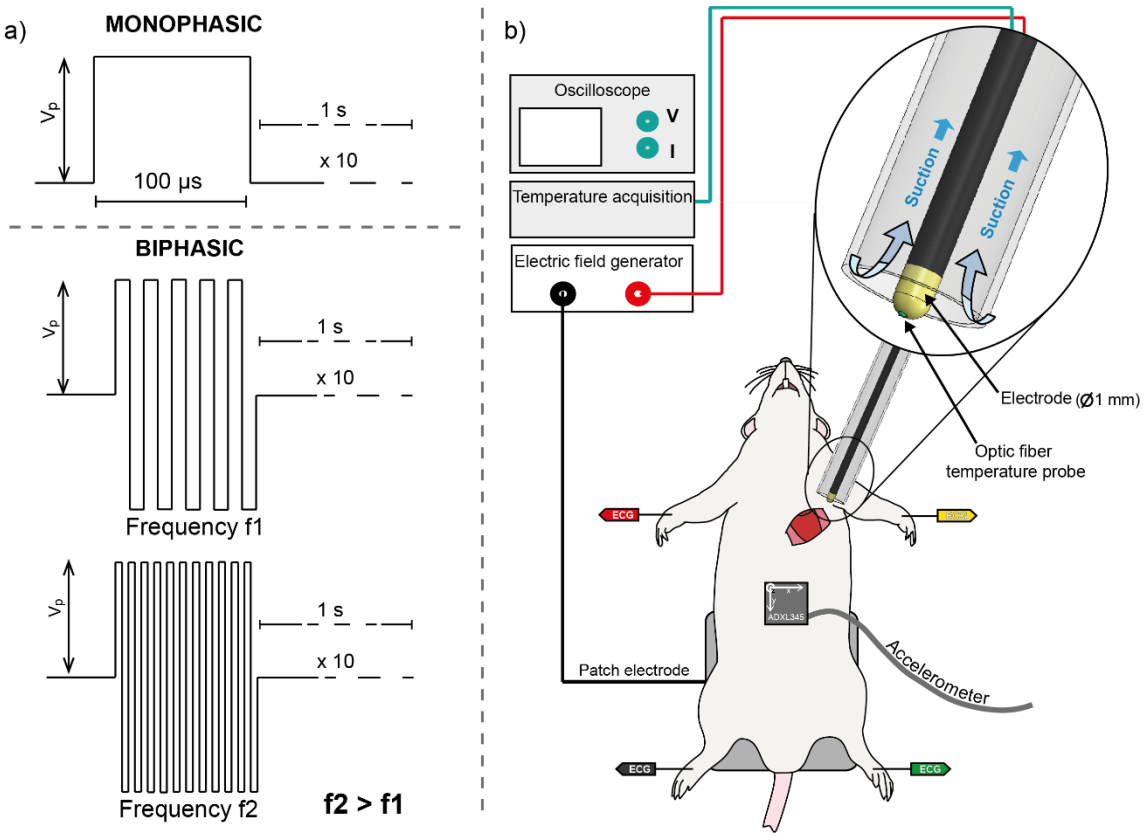

Fig. 1 a) Schematic representation of the monophasic square pulse treatment (upper part) and two examples of the biphasic treatment representing two different frequencies (lower part). As shown, each complete treatment consisted in applying 10 pulses/bursts of 100 µs duration, at a repetition rate of 1 per second (total treatment duration of 10 s). b) Diagram of the setup used for the in vivo experiments. The magnification shows in detail the monopolar electrode and suction system used to apply EF to cardiac tissue, return electrode was a patch electrode attached to the back of the animals. An optic fiber temperature probe was placed inside the electrode to measure temperature changes in the interface between electrode and heart tissue. To measure muscle contractions an accelerometer was attached to the abdomen of the animals. The surface ECG was continuously recorded.

PFA was applied in a monopolar way to the left ventricle of an open chest rat model. The exposure setup consisted of a tip electrode that was placed perpendicular to the epicardial surface (medial/base ventricle level) and a patch electrode (half pad of 3M^{TM} 9160F) attached the lower back of the animals. The gold-plated tip electrode had 1 mm diameter, 1.5 mm height and was mounted in a plastic tube that enabled applying mild suction when the electrode was positioned against the epicardium. Given the strong movements of a beating heart, a suction system was used to ensure a correct and constant contact during PFA application. The level of suction pressure was carefully selected through a manometer connected to a vacuum pump to avoid any damage to the tissue. In Fig. 1b detailed representation of the exposure system is depicted.

The high-frequency square biphasic electroporation (EP) pulses, were generated by a custom made generator based on a modular structure [19]. A different custom-made generator was used to generate the 100 μs monophasic square pulses.

In order to accurately measure, the temperature rise during PFA application, a temperature fiber optic sensor based on GaAs (gallium arsenide) technology was used (bare tip sensor THR-NS-1165C, FISO Technologies, INC, Canada). The optic fiber sensor (diameter 243 μm) was inserted throughout a hole in the center of the metallic tip electrode. Thus, the active part of the sensor was placed right on the cardiac tissue/electrode interface (see Fig. 1b detail). Temperature was acquired at a sampling rate of 125 Hz.

Surface ECG was continuously recorded using a CardioSoft system (GE Healthcare, Germany) at a sampling rate of 200 Hz. Transient ECG distortion was produced during PFA applications and recovered back immediately after. Changes in the amplitude and duration of the P-wave, QRS-complex duration, RR-interval and ST segment at the J point were measured with Matlab scripts at ECG lead II. Lead II was selected because the voltage signal of this lead was less affected after the left-thoracotomy. The measurements were taken at baseline, immediately before and after the PFA procedure, 30 min after the PFA procedure, and 3-weeks after.

The induction of muscle contractions by the ELF delivery was monitored during the treatments by means of a 3-axis digital accelerometer (ADXL345, Analog Devices, Inc., USA) mounted on a printed circuit board that was fixed to the animal abdomen 1 cm below the sternum.

Voltage and current were monitored during PFA applications using a digital oscilloscope (Rohde & Schwarz RTB2004), a high voltage probe (Tektronix P5100 A) and current probe (Tektronix TCP2020).

Animal study protocol

The study protocol was approved by the Animal Care and Use Committee of the Hospital de la Santa Creu i Sant Pau (HSCSP) and conformed to the *Guide for the Care and Use of Laboratory Animals*, 8th edition (National Research Council, The National Academies Press, Washington, DC, 2010). Animals were housed in the animal facilities of HSCSP in a dedicated room with controlled temperature, humidity, and lighting.

Twenty-nine Sprague-Dawley rats (≈50% sex ratio) (Charles River Laboratories, France) with average weight of 290±70 grams were used in this study. Treatments were performed after a one-week acclimation period. Before treatment, animals were anesthetized using a subcutaneous injection of a mixture of ketamine (75mg/kg) and xylacine (10mg/kg). Following, endotracheal intubation was performed and mechanical ventilation was maintained at a rate of 75 breaths/minute. General anesthesia was maintained with a mixture of oxygen and isoflurane inhalation (1%–2%). The surface ECG was continuously monitored and acquired throughout the whole procedure. A surgical window was created by a left thoracotomy to gain access to the epicardial surface as previously described [17,18] and the return patch electrode was fixed to the lower back of the animal in a previously shaved area. The monopolar electrode was positioned on the epicardium of the lateral wall of the left ventricle. Subsequently, a baseline recording of all variables was initiated and then the PFA was applied. All experiments were videorecorded. After the PFA procedure, thorax and skin were closed and sutured, animals were extubated and recovered from anesthesia, and housed for a follow-up period of 21 days. After this period, animals were anesthetized as in the first intervention, a surface ECG recorded, and then the animals were euthanized by cervical dislocation. Immediately after, the beating heart was explanted, washed in physiological 0.9 % NaCl solution and immersed in a 4 % paraformaldehyde solution for fixation for at least 48 hours before further processing.

Histological analysis

Fixed heart tissue was embedded in paraffin blocks for histological analysis. Sequential sections of 4 μm thickness, acquired every 60 μm from base to apex around the lesion area, were mounted and stained with Masson's trichrome. Digital images of the stained sections were acquired using a PANNORAMIC MIDI digital scanner (3DHistech). Morphometric measurements were performed for each animal in the histological section displaying the largest fibrotic lesion ((corresponding with the center of the lesion). Lesion depth and width were estimated using open-source software QuPath. Briefly, for each sample the ellipse that best fitted the lesion shape was manually depicted and depth from the center and width at the intersection of the ellipse with the epicardium were measured. Subsequently, lesion area was estimated after manually depicting the exact lesion contour.

The identification of additional histological changes (blinded groups) was done by direct visualization of the histological preparation by an expert pathologist at proper magnification.

Computer simulations

Computational models are used to measure the ELF intensity because it cannot be directly measured during PFA treatments. Numerical simulations were used to calculate the ELF magnitude distribution and the collateral heating produced by each setup used in the in vivo experiments. Then, the ELF thresholds necessary to cause IRE were estimated by direct comparison with histological morphometric results obtained from experiments for each condition. The same ELF delivery parameters used in the experiments were modelled, i. e., monophasic square pulses and high-frequency biphasic bursts at the different frequencies studied and voltages applied.

The model was built using the finite element method (FEM) software COMSOL Multiphysics 5.3 (COMSOL AB, Stockholm, Sweden) using the AC/DC module to calculate the ELF distribution and the Heat transfer module for the temperature changes during the ELF delivery. The modeled

geometry consisted of a 3D reconstruction of the ventricles of the rat (atria were neglected due to their very small size) and the monopolar electrode setup. The 3D reconstruction of the ventricles was built from histological sections corresponding to the region where the electrode was positioned. The body of the rat was approximated by a rectangular volume with dimensions similar to the length and width of the animals studied (14 × 6 cm) and a patch electrode at the bottom. To mimic the effect of the pressure that the electrode exerts on the epicardial surface, the tip of the electrode was placed at a penetration depth of 0.75 mm. See supplementary section S2 for a detailed view of the modelled geometry.

The numerical model simultaneously solved the electric potential, the temperature and the electrical conductivity (σ) distributions in the treatment region during ELF application using the coupled physics feature of COMSOL in a time dependent study. A full description of the methods used to implement the model are provided in Supplementary Information.

After the in vivo experiments, IRE ELF thresholds were estimated for every treatment condition. The ELF threshold was calculated in a cut plane of the 3D geometry, similar to the cut plane where histological sections were analyzed. Threshold values were extracted as the levels that provided an integral surface equal to the mean lesion area obtained in vivo.

Statistical analysis

Continuous variables were reported as the mean ± standard deviation (SD). Significance of differences for histological morphometric measurements was assessed between groups corresponding to the same EP voltage using a one-way ANOVA analysis. When group differences were found ($p<0.05$), the one-way ANOVA was followed by pairwise comparisons of groups, and the probability values were adjusted for multiple comparisons using the Bonferroni correction. Statistical analysis was performed with IBM SPSS (v. 26).

Results

Effect of waveform frequency on in vivo PFA lesion formation

A total of twenty-nine rats were treated with monophasic or biphasic waveforms of different frequencies and two voltage levels (500 V and 800 V) with one epicardial application site per rat (n=4-5 rats per group). Only one animal from the monophasic group died immediately after the PFA treatment, the rest of animals survived without complications. Although PFA applications were not synchronized with the ECG, no ventricular nor atrial arrhythmias were detected in any case.

The histological study of the tissues three weeks after treatment shows a clear dependence on the frequency and amplitude of the ELF for lesion formation. For biphasic waveforms, a clear loss on PFA efficacy can be observed with increasing frequency (see Fig. 2a for representative examples of histological sections stained with Masson's Trichrome for each studied group). A similar frequency dependence was observed in the in vitro study performed previous to the in vivo experiments (see Supplemental Materials).

Morphological measurements show that at voltage of 500 V, for all frequencies, the monophasic pulses create the biggest lesions. For this same voltage, mean depth, width and surface of lesions are significantly reduced when biphasic bursts are applied. When frequency is increased, lesions dimensions are clearly reduced. Significant differences are found in lesion depth, width and surface between the 90 kHz and 450 kHz groups. It is worth noting that in some animals at 450 kHz lesions are very small, almost negligible. When voltage is increased to 800 V, a clear increase in lesion size with respect to 500 V is observed for all frequencies. In fact, the increase of voltage to 800 V for the biphasic bursts at 90 kHz, created similar lesion dimensions to the lesions created by the 500 V monophasic pulses. Again, a gradual loss of PFA efficacy is observed for increasing frequencies with significant differences in surface and width between 90 kHz and 450 kHz. In Fig. 3 the morphological measurements are graphically represented for all conditions studied. In Table 1, the same values (mean ±SD) are detailed.

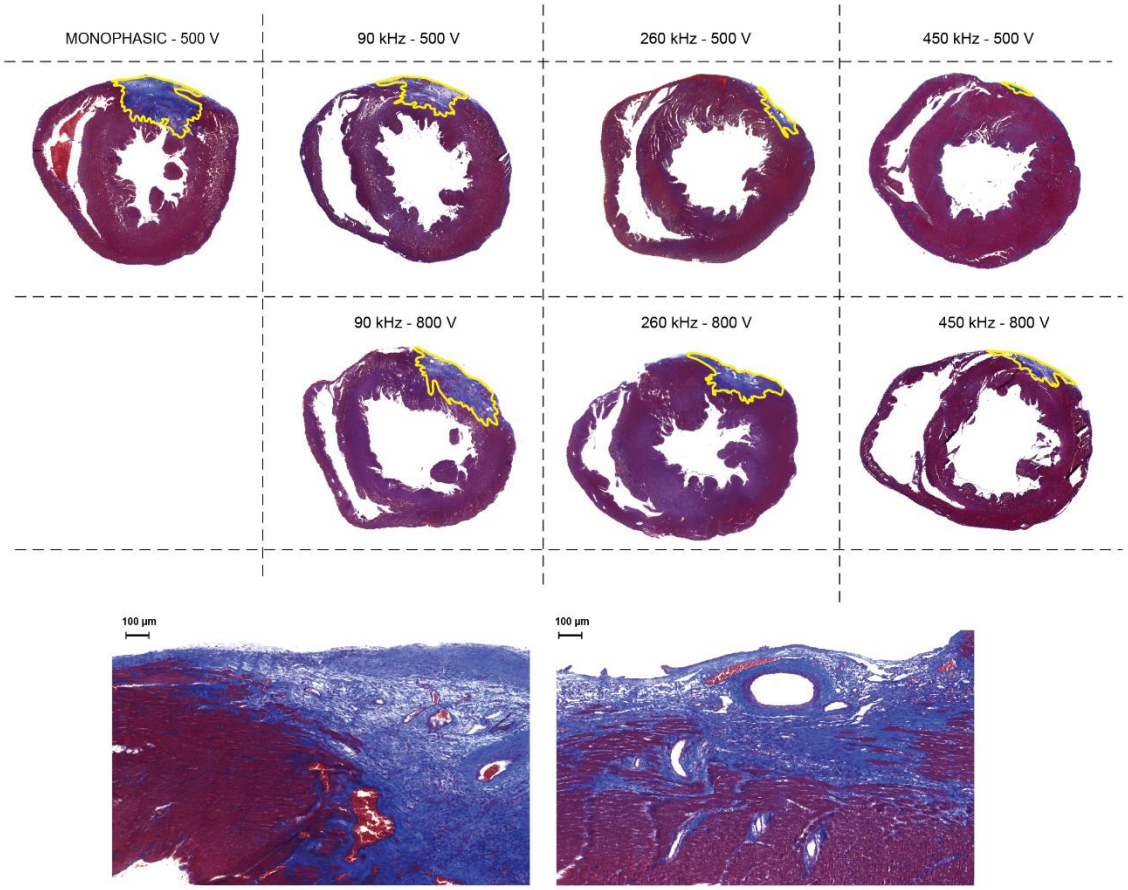

Fig. 2 Representative examples of histological sections corresponding to cuts at the center of the PFA lesions for the different experimental groups. Samples were stained with Masson's Trichrome three weeks after treatment. In the lower insert two representative lesions are shown at higher magnification; left corresponds to monophasic at 500 V, right corresponds to biphasic at 260 kHz and 800 V (scale bar corresponds to 100 µm).

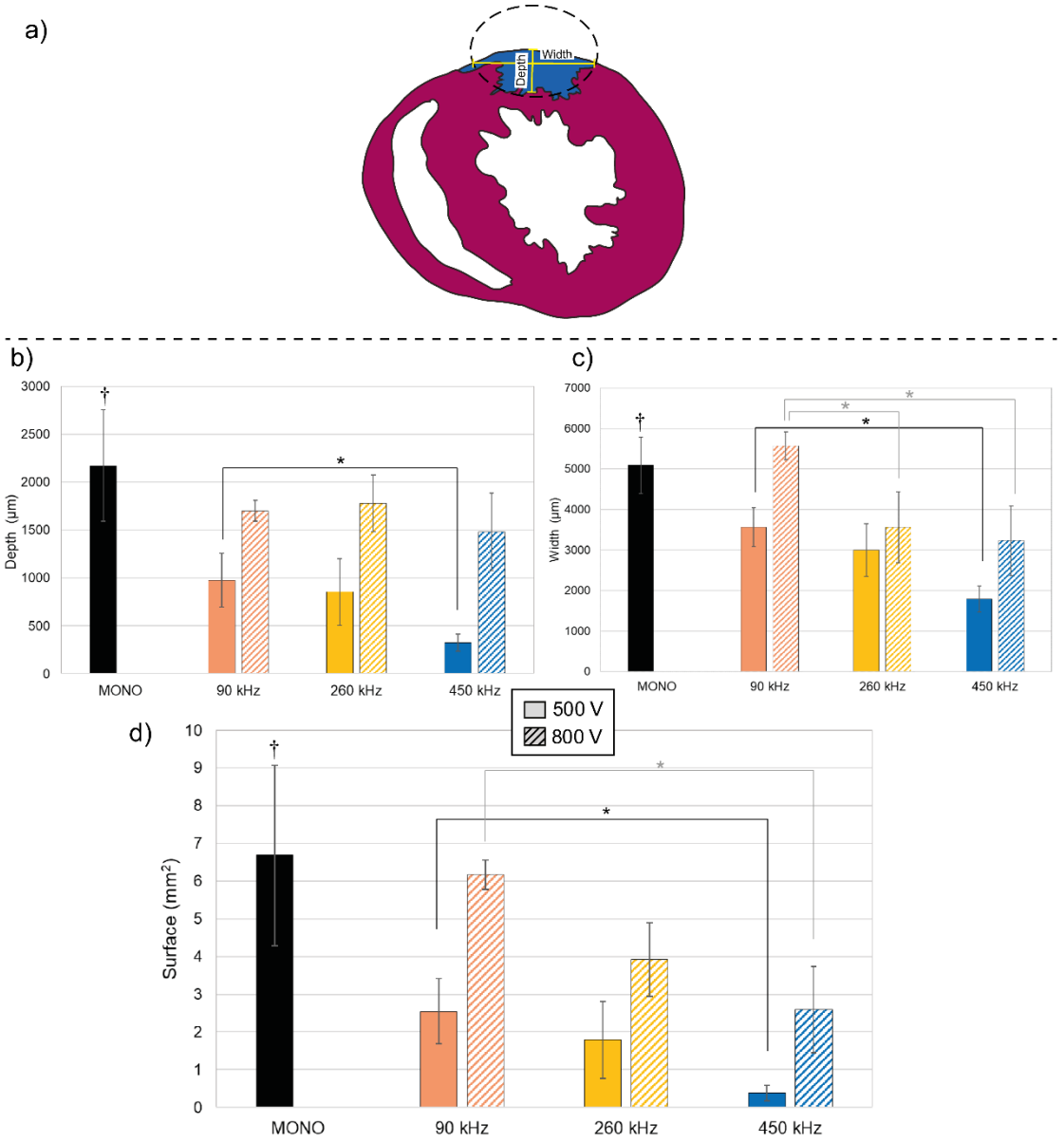

Fig. 3 Morphometric measurements. a) Schematic explanation of the different measurements acquired. b), c) and d) show mean lesion depth, width and surface, respectively, for the different experimental groups. For biphasic waveforms, values are shown for the two voltage levels assayed (500 and 800 V). Values are reported as the mean ± standard deviation. * significant at $p<0.05$ (comparison between biphasic groups at the same voltage). † significant at $p<0.05$ (comparison between monophasic group and biphasic groups at 500 V).

Lesions dimensions

PFA condition		Depth (mm)	Width (mm)	Surface (mm^2)
500 V	90 kHz	0.97±0.27	3.56±0.47	2.55±0.86
	260 kHz	0.85±0.34	3.00±0.64	1.78±1.02
	450 kHz	0.32±0.08	1.79±0.32	0.38±0.20
	Monophasic	2.17±0.58	5.08±0.69	6.67±2.39
		* p<0.05	* p<0.05	* p<0.05
800 V	90 kHz	1.70±0.11	5.81±0.22	6.17±0.38
	260 kHz	1.78±0.07	3.56±0.40	3.91±0.98
	450 kHz	1.48±0.40	3.13±0.85	2.59±1.14
		p=0.56	* p<0.05	* p<0.05

Table 1 Summary of morphometric measurements. Values are reported as mean ±SD. p-values from the one-way ANOVA.

Induction of muscle contractions

Accelerometer measurements show a clear dependence with frequency (see Fig. 4). For 500 V, a clear reduction in the intensity of contractions is observed when frequency is increased from 90 kHz to 260 kHz. For 800 V, the reduction observed, although less pronounced is observed when frequency is increased from 260 kHz to 450 kHz. No differences were found between monophasic pulses at 500 V and 90 kHz biphasic bursts at 500 V or 800 V. Examples of videos for different contraction levels are available in Supplementary data.

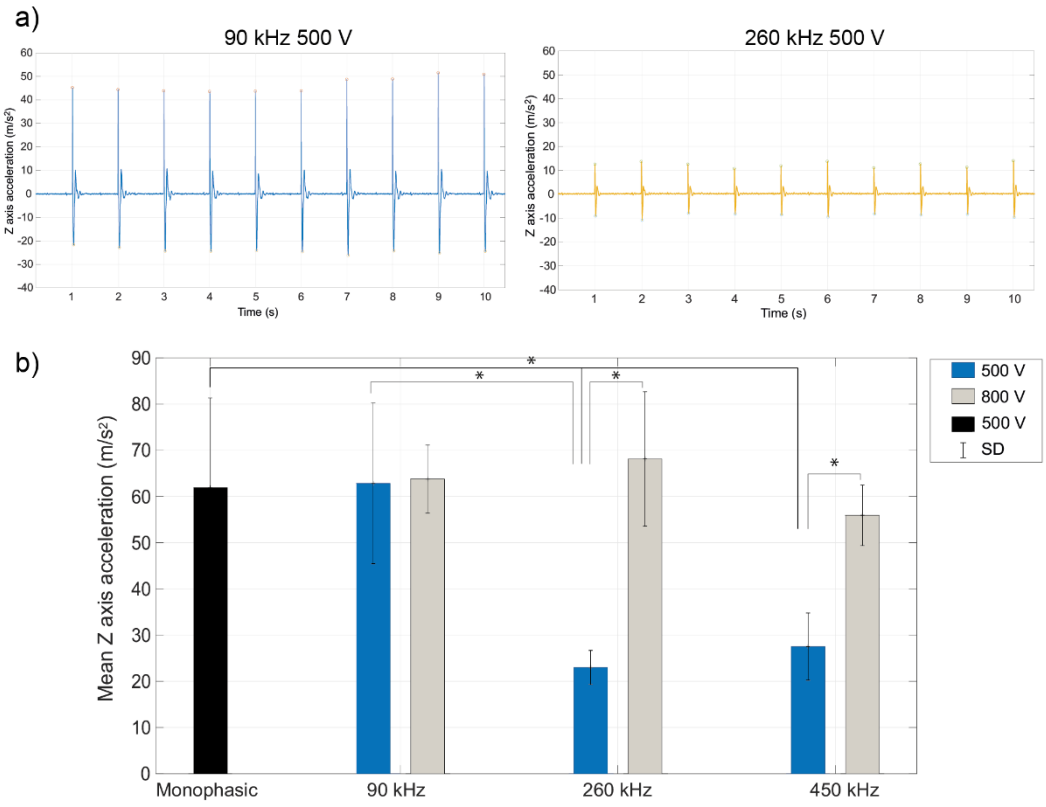

Fig. 4 Accelerometer recordings of collateral muscle contractions intensity. a) Examples of Z axis acceleration during a complete treatment sequence for two different conditions with the same voltage (500 V) but different frequencies (90 and 260 kHz). b) Quantification of mean z axis acceleration for all experimental groups. Data is shown as the mean ±SD. * significant at $p<0.05$

Temperature recordings

The temperature measurements show, for the first time in PFA research, how temperature sharply increases at the application site during each EP burst (max $\Delta T \approx 1.5$ °) and subsequently decreases with slower dynamics between consecutive bursts. Maximum absolute temperature increase registered along a complete treatment was ≈ 3 °C (see Fig. 5). Temperature was recorded at the point of contact between the electrode tip and the tissue surface, where the ELF intensity is maximum and thus, the heating is also maximum. Thermal simulations using the computational model previously shown provided very similar temperature dynamics but higher maximum temperature values, still far from thermal damage (see Supplemental Materials). These results

demonstrate that the effects observed in tissue cannot be the result of thermal injury, confirming the non-thermal nature of the obtained PFA lesions in this study.

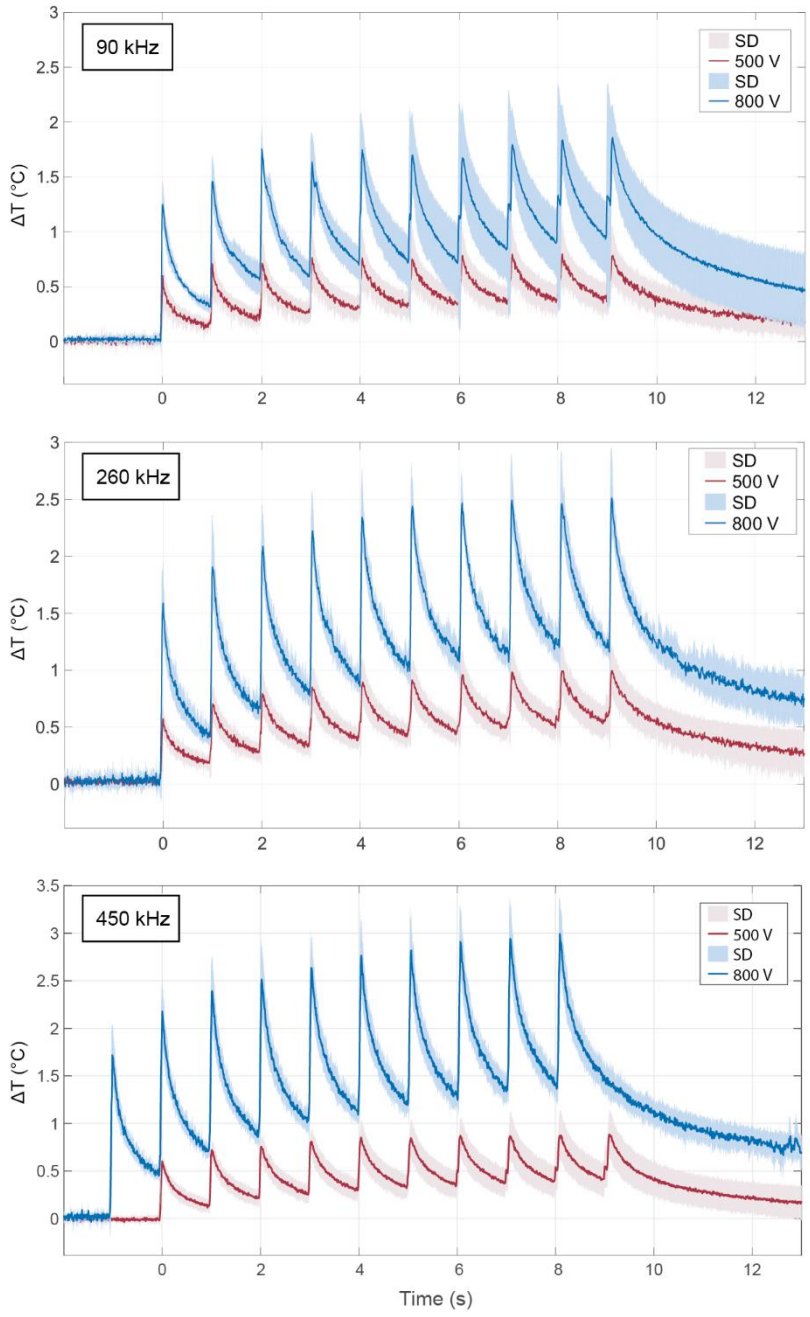

Fig. 5 Temperature variation at the application electrode surface. Mean temperature variation (solid lines) ± SD (shadow areas) for each experimental biphasic group is shown during the complete treatment sequences for the two voltage levels studied; 500 V (red) and 800 V (blue). Recordings for the monophasic pulses displayed a very similar behavior (data not shown).

Histopathological observations

Observation of the trichrome-stained histological sections by an expert pathologist confirmed fibrosis in the blue-stained areas with preserved structure in arterioles, venules and the rest of medium diameter vessels (see high magnification examples in **¡Error! No se encuentra el origen de la referencia.** lower panels). Lesions displayed homogeneous fibrosis with no evidence of tissue sparing around blood vessels (no effect of blood flow cooling). Signs of perivascular chronic inflammation were observed in some instances at the subepicardial level. In some lesions, small surviving cardiomyocytes cores were observed in the periphery of the lesions. Most lesions presented relatively well-defined borders with some areas of jagged borders and fibrotic infiltration.

Numerical estimation of irreversible electroporation lethal thresholds

The solution of the electric field intensity distribution provided by the numerical model predicts a semi-ellipsoidal high ELF intensity region in the left ventricle epicardium around the electrode tip. This distribution is very similar to the actual shape of the lesions obtained in the in vivo experiments (see Fig. 6a and Fig. 6b for examples of the predicted ELF distribution).

The ELF lethal thresholds calculated from comparison between the real lesions and the model confirm the frequency dependence observed. Notice that because the small size of the lesions obtained with biphasic bursts of 450 kHz and 500 V, the ELF lethal threshold was not calculated for this condition. For monophasic pulses, the threshold value obtained is 640 V/cm, for 450 kHz the threshold obtained is 2050 V/cm. For 90 kHz and 260 kHz the threshold is reported as a range corresponding to the threshold levels obtained for 500 V and 800 V, respectively. For 90 kHz the threshold value ranges from 1025-1300 V/cm and for 260 kHz from 1420-1690 V/cm. Threshold values against frequency are depicted in Fig. 6c.

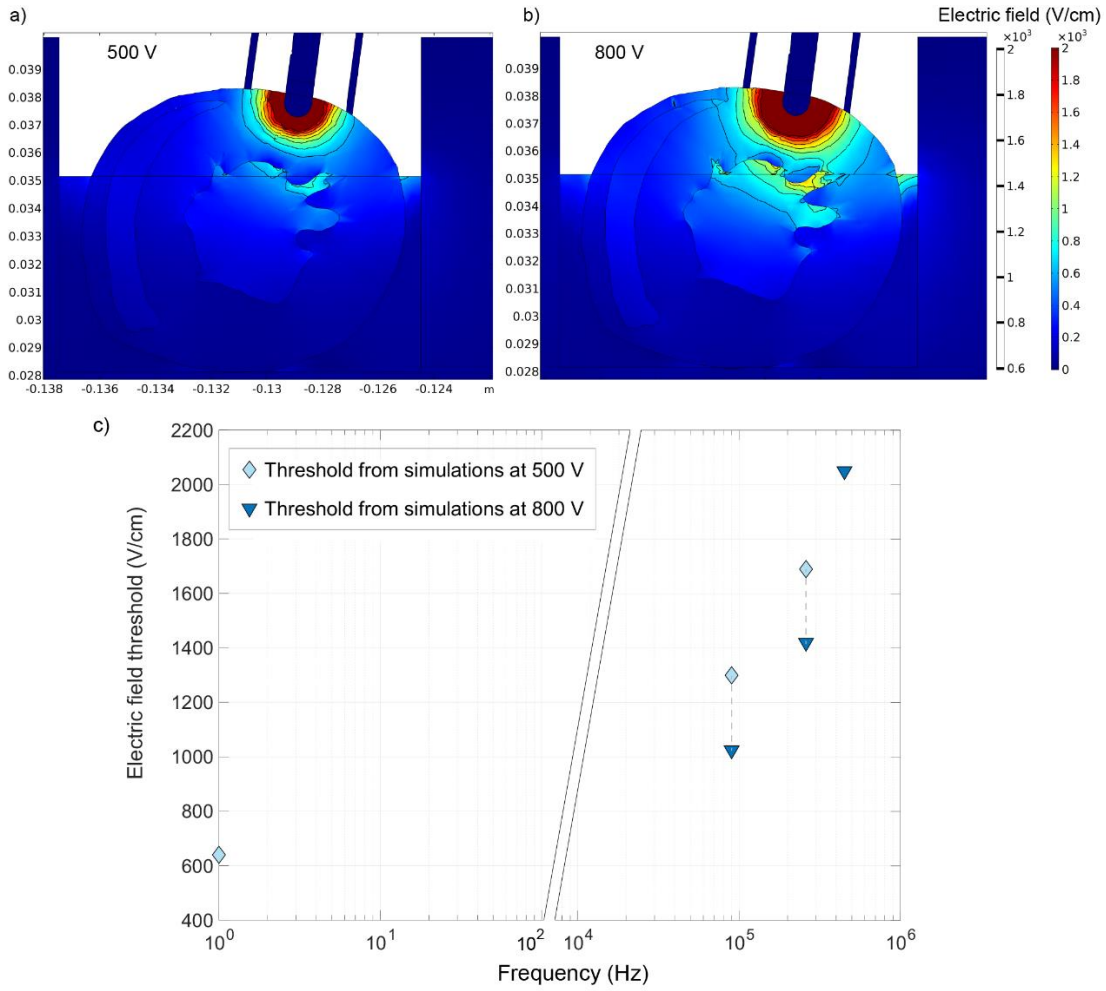

Fig. 6 Computer simulation results. a) and b) Example of electric field intensity distribution (colors) and electric field isolevel lines for simulations at 500 V and 800 V, respectively. The data corresponds to simulations at 90 kHz. Data is shown in a cut plane of the 3D heart geometry at the middle of the electrode. For convenience, upper color scale is saturated for EF intensities higher than 2000 V/cm. c) EF lethal thresholds obtained from comparison between experimental in vivo lesions and computer simulations for every group. Note that for 90 kHz and 260 kHz threshold is represented as a range between the value obtained at 500 V and the value obtained at 800 V. Note that monophasic pulses are plotted in the low frequency range (considered quasi-DC waveform).

Discussion

This study has examined the role of the frequency of biphasic waveforms on PFA efficacy in healthy ventricular myocardium of rats using a monopolar electrode. Additionally, the study compared the efficacy of PFA biphasic vs. monophasic waveforms while directly measuring neuromuscular contractions and temperature increase at the tissue-electrode interface.

Compared to prior preclinical studies, the present work systematically reports for the first time a correlation between waveform configuration and lesion dimensions with a monopolar electrode. The novelty of the study resides in the multimethodological approach combining in vitro experiments with cells, numerical models, and in vivo experiments.

Main findings

1. Biphasic PFA exhibits a clear dependency on the frequency of the waveform: lesion dimensions decrease with increasing frequency. Monophasic waveforms yielded the largest lesions.
2. For the first time, this study reports the actual electric field lethal thresholds necessary for cardiac PFA in vivo and their dependence with the characteristics of the waveform used.
3. Collateral neuromuscular stimulation depends on the waveform frequency: stimulation probability decreases with increasing frequency. Tissue heating is very low and relatively independent of waveform frequency.

Monophasic vs. biphasic pulses

Our results confirm a clear loss of PFA efficacy when biphasic pulses are used instead of monophasic pulses. However, for the lowest biphasic frequency (90 kHz), similar lesions to the monophasic pulses can be obtained by increasing the voltage applied from 500 V to 800 V.

Previous studies have shown that despite the loss in electroporation efficacy with biphasic waveforms, their main advantage in IRE treatments is based on the reduction or complete

elimination of collateral stimulation of nerve fibers leading to muscle contractions or pain[20–22]. In PFA clinical practice this could prevent the need for muscle relaxants, analgesics or deep anesthesia. Another major advantage of biphasic waveforms is the reduction or complete elimination of electrochemical reactions at the electrodes surface and the associated gas bubbles formation [23,24], thus minimizing the risk of gas emboli. Furthermore, IRE energy delivery has the potential risk of inducing cardiac arrhythmias [25,26]. Recent studies have reported the use of unsynchronized PFA treatments using biphasic pulses with no adverse effects [7,27].

Frequency dependence

The observed frequency dependence of PFA on cardiac tissue has been previously reported for other tissues in the frame of IRE cancer ablation [22,28,29]. Its mechanism is based on a bioelectric phenomenon: as frequency increases, the external ELF gradually losses its ability to induce a sufficiently high transmembrane potential to initiate the EP phenomenon[29]. Remarkably, the electrical stimulation of excitable cells also depends on inducing a transmembrane potential. This is why, when frequency increases, reduced muscle contractions are observed[30]. However, EP seems to be less sensitive to frequency than nerve stimulation[31].

The results of the in vitro experiments performed (see Supplemental Material) show that equivalent PFA efficacy can be found by balancing waveform frequency and ELF magnitude. Note that IRE thresholds extracted from these in vitro experiments may substantially differ from actual values required in vivo[32–34], and therefore, these values should not be extrapolated in vivo. The optimal frequency for a PFA clinical treatment would be that at which there is trade-off between reduction in collateral effects and efficacy. Concerning stimulation, the higher the frequency the better. However, increasing the frequency would require applying higher ELF intensities. This would result in a marked increase in the risk of unwanted tissue thermal injury and electrical safety issues. Another alternative is to increase the number of consecutive applications [16–18]. However, this approach has limitations since the relation is not linear and the increase in the number of applications reaches a plateau in the observed effect[35].

Finally, cell death induced by EP is a complex phenomenon where different pathways as apoptosis, necrosis, necroptosis, and pyroptosis have been described [36,37]. Previous studies have shown significant differences in the dominant cell death pathway depending on the waveform used [38–40]. The frequency of the biphasic waveform could play an important role to reduce excessive inflammatory response and promote apoptosis, but this is a hypothesis that warrants further research.

Electric field lethal thresholds

As far as we know, this is the first time that ELF lethal threshold values are reported in vivo for cardiac PFA. Our results show a considerable non-linear increase of lethal threshold with frequency. The interest of extracting EP thresholds for specific waveform configurations resides in two main aspects: i) once the thresholds are obtained, it could be possible to make a better comparison between the results obtained with different clinical PFA platforms, which use different waveform configurations; ii) computational models can be used as treatment planning tools to optimize the voltage applied or the position of an specific catheter to obtain a desired lesion size[41]. As we demonstrate, ELF lethal threshold depends on waveform configuration and each one has its own ELF lethal threshold. Thus, the use of an universal PFA threshold value, as reported in previous studies,[42] does not seem appropriate.

Collateral effects

We show that muscle contractions are considerably reduced with higher frequencies. However, they do not completely disappear even at 450 kHz, what is unexpected when comparing to previous experiences [20,22,43] . We believe that a possible explanation for this finding, not clearly reported in comparable pre-clinical and clinical setups [15,44,45], is the relative size of the electrode compared to the size of the treated animal. We intentionally decided to use a relatively big electrode to allow a correct visualization of the lesions during analysis. As a drawback, it probably hampered the complete elimination of muscle contractions. The question whether with a high

enough frequency it is possible to completely eliminate surrounding neuromuscular capture while preserving PFA efficacy is not solved with our observations. We expect that with a realistic electrode/tissue scale, it should completely disappear at high frequency.

Regarding collateral heating, our measurements demonstrate how, even for very short application durations (100 µs) separated by a long delay (1 second), a non-negligible rise in temperature is produced at the tissue-electrode interface which is relatively independent of the waveform frequency. This finding remarks the risk of thermal damage related to PFA. This highlights its importance in optimal waveform design and the need of reporting local temperature during PFA applications.

Finally, despite that the PFA applications were not synchronized with the ECG, we did not trigger any ventricular or supraventricular arrhythmia. It has been previously shown for monophasic pulses in cancer electroporation that the risk of arrhythmia induction when applications were not synchronized with the heart was non-negligible[25,46]. Other PFA studies have reported the absence of arrhythmia induction during unsynchronized biphasic applications, but they used bipolar electrodes that confine the ELF to a small region [7,47]. We safely used, without arrhythmia induction, a relatively large monopolar electrode directly applied on the ventricle However, this could substantially differ in larger animal models with a lower heart rate and should be further studied to establish the safety limits of unsynchronized applications in PFA.

Limitations

This is an animal study performed in the healthy myocardium of a rat model and the exact values of the electric field levels could differ to the values required in clinical applications. However, the dependencies provided in this study can be used later for exploring the optimal waveform configuration in human tissue. Second, electric field was applied epicardially in an open chest model what it is not the preferred approach in clinical practice. Additionally, the amount and distribution of epicardial fat could differ between species. However, the methodology used allowed a perfect control of the position and contact of the catheter, assuring the fidelity of the

applications. Finally, the relation between electrode size and applied voltage in this study was intentionally selected to create measurable lesions of limited transmurality. Therefore, the maximum lesions depths obtained (about 2-3 mm) cannot be translated to a bigger animal model or humans. In order to assess complete tissue depths, a large animal model should be used.

Conclusions

Most of clinical and preclinical systems for PFA use biphasic electric waveforms for electric field delivery. In this study we demonstrate how the frequency of the biphasic waveforms plays a key role in determining treatment efficacy and collateral muscle contractions. As shown, the lethal threshold for electroporation highly depends on the characteristics of the applied waveform with threshold ranging from around 600 V/cm for monophasic waveforms to near 2000 V/cm for biphasic waveforms with a frequency of 450 kHz. This highlights the difficulty to perform an adequate comparison between different clinical PFA systems and the need of waveform reporting and/or standardization. These results warrant future studies in experimental models closer to the final clinical application.

Acknowledgements

We would like to thank Mario Gomez Barea for his support during experiments. We would also like to thank Elena Serrano Carballal for her advice during histological sample processing.

Sources of Funding

This work was partially supported by project (PID2019-110120RBI00/AEI/ 10.13039/501100011033) from the Ministry of Science, Innovation and Universities and the State Research Agency of the Spanish government. This project has received funding from the European Union's Horizon 2020 research and innovation program under the Marie Skłodowska-Curie grant agreement No 892393 (TACAIRE). Antoni Ivorra gratefully acknowledges financial support by ICREA under the ICREA Academia program.

Disclosures

Dr. García-Sánchez is a consultant for Argá Medtech SA and Medlumics SL. Dr. Guerra has served as consultant for Biosense Webster, Boston Scientific and Abbott, received speaker fees from Boston Scientific and Abbott, and received a research grant from Abbott and Medtronic. Dr Ivorra is a consultant for Argá Medtech SA and Medlumics SL.

Supplemental Material

List of Supplemental Materials

- Supplemental Information
- Videos 1-4
- References 48–57

References

1. Maor E, Sugrue A, Witt C, et al. Pulsed electric fields for cardiac ablation and beyond: A state-of-the-art review. *Hear Rhythm*. 2019;16(7):1112-1120. doi:10.1016/j.hrthm.2019.01.012

2. Sugrue A, Vaidya V, Witt C, et al. Irreversible electroporation for catheter-based cardiac ablation: a systematic review of the preclinical experience. *J Interv Card Electrophysiol*. 2019;55(3):251-265. doi:10.1007/s10840-019-00574-3

3. Berruezo A, Penela D. Witnessing the birth of the future's ablation therapy? *Europace*. 2020;22(3):340-341. doi:10.1093/europace/euaa019

4. Bradley CJ, Haines DE. Pulsed field ablation for pulmonary vein isolation in the treatment of atrial fibrillation. *J Cardiovasc Electrophysiol*. 2020;31(8):2136-2147. doi:10.1111/jce.14414

5. Verma A, Asivatham SJ, Deneke T, Castellvi Q, Neal RE. Primer on Pulsed Electrical Field Ablation: Understanding the Benefits and Limitations. *Circ Arrhythmia Electrophysiol*. 2021;(September):1-16. doi:10.1161/CIRCEP.121.010086

6. Sugrue A, Maor E, Ivorra A, et al. Irreversible electroporation for the treatment of cardiac arrhythmias. *Expert Rev Cardiovasc Ther*. 2018;16(5):349-360. doi:10.1080/14779072.2018.1459185

7. Reddy VY, Dukkipati SR, Neuzil P, et al. Pulsed Field Ablation of Paroxysmal Atrial Fibrillation: 1-Year Outcomes of IMPULSE, PEFCAT, and PEFCAT II. *JACC Clin Electrophysiol*. 2021;7(5):614-627. doi:10.1016/j.jacep.2021.02.014

8. Weaver JC, Smith KC, Esser AT, Son RS, Gowrishankar TR. A brief overview of electroporation pulse strength-duration space: A region where additional intracellular effects are expected. *Bioelectrochemistry*. 2012;87(0):236-243. doi:http://dx.doi.org/10.1016/j.bioelechem.2012.02.007

9. Miklovic T, Latouche EL, DeWitt MR, Davalos R V., Sano MB. A Comprehensive Characterization of Parameters Affecting High-Frequency Irreversible Electroporation Lesions. *Ann Biomed Eng*. 2017;45(11):2524-2534. doi:10.1007/s10439-017-1889-2

10. Flisar K, Puc M, Kotnik T, Miklavcic D. Cell membrane electropermeabilization with arbitrary pulse waveforms. *IEEE Eng Med Biol Mag*. 2003;22(1):77-81. doi:10.1109/MEMB.2003.1191453

11. Arena CB, Sano MB, Rylander MN, Davalos R V. Theoretical considerations of tissue

electroporation with high-frequency bipolar pulses. *IEEE Trans Biomed Eng*. 2011;58(5):1474-1482. doi:10.1109/TBME.2010.2102021

12. Stewart MT, Haines DE, Verma A, et al. Intracardiac Pulsed Field Ablation: Proof of Feasibility in a Chronic Porcine Model. *Hear Rhythm*. 2018. doi:10.1016/j.hrthm.2018.10.030

13. Van Es R, Konings MK, Du Pré BC, et al. High-frequency irreversible electroporation for cardiac ablation using an asymmetrical waveform. *Biomed Eng Online*. 2019;18(1):1-13. doi:10.1186/s12938-019-0693-7

14. Loh P, Van Es R, Groen MHA, et al. Pulmonary vein isolation with single pulse irreversible electroporation: A first in human study in 10 patients with atrial fibrillation. *Circ Arrhythmia Electrophysiol*. 2020:1083-1091. doi:10.1161/CIRCEP.119.008192

15. Caluori G, Odehnalova E, Jadczyk T, et al. AC Pulsed Field Ablation Is Feasible and Safe in Atrial and Ventricular Settings: A Proof-of-Concept Chronic Animal Study. *Front Bioeng Biotechnol*. 2020;8(December). doi:10.3389/fbioe.2020.552357

16. Yavin HD, Higuchi K, Sroubek J, Younis A, Zilberman I, Anter E. Pulsed-Field Ablation in Ventricular Myocardium Using a Focal Catheter: The Impact of Application Repetition on Lesion Dimensions. *Circ Arrhythmia Electrophysiol*. 2021. doi:10.1161/CIRCEP.121.010375

17. Zager Y, Kain D, Landa N, Leor J, Maor E. Optimization of irreversible electroporation protocols for in-vivo myocardial decellularization. *PLoS One*. 2016;11(11):1-15. doi:10.1371/journal.pone.0165475

18. Heller E, Garcia-Sanchez T, Moshkovits Y, et al. Comparing High-Frequency With Monophasic Electroporation Protocols in an In Vivo Beating Heart Model. *JACC Clin Electrophysiol*. 2021;7(8). doi:10.1016/j.jacep.2021.05.003

19. Sarnago H, Lucia O, Naval A, Burdio JM, Castellvi Q, Ivorra A. A Versatile Multilevel Converter Platform for Cancer Treatment Using Irreversible Electroporation. *IEEE J Emerg Sel Top Power Electron*. 2016;4(1):236-242. doi:10.1109/JESTPE.2015.2512324

20. Sano MB, Fan RE, Cheng K, et al. Reduction of Muscle Contractions during Irreversible Electroporation Therapy Using High-Frequency Bursts of Alternating Polarity Pulses: A Laboratory Investigation in an Ex Vivo Swine Model. *J Vasc Interv Radiol*. 2018;29(6):893-898.e4. doi:10.1016/j.jvir.2017.12.019

21. Arena CB, Sano MB, Jr JHR, et al. High-frequency irreversible electroporation (H-FIRE) for non-thermal ablation without muscle contraction. *Biomed Eng Online*.

2011;10(1):102. doi:10.1186/1475-925X-10-102

22. Castellví Q, Mercadal B, Moll X, Fondevila D, Andaluz A, Ivorra A. Avoiding neuromuscular stimulation in liver irreversible electroporation using radiofrequency electric fields. *Phys Med Biol*. 2018;63(3):35027. http://stacks.iop.org/0031-9155/63/i=3/a=035027.

23. Pataro G, Donsì G, Ferrari G. Modeling of electrochemical reactions during pulsed electric field treatment. In: *Handbook of Electroporation*. Vol 2. ; 2017. doi:10.1007/978-3-319-32886-7_5

24. Kotnik T, Miklavcic D, Mir LM. Cell membrane electropermeabilization by symmetrical bipolar rectangular pulses. Part II. Reduced electrolytic contamination. *Bioelectrochemistry*. 2001;54(1):91-95.

25. Thomson KR, Cheung W, Ellis SJ, et al. Investigation of the safety of irreversible electroporation in humans. *J Vasc Interv Radiol*. 2011;22(5):611-621. doi:10.1016/j.jvir.2010.12.014

26. Mali B, Jarm T, Corovic S, et al. The effect of electroporation pulses on functioning of the heart. *Med Biol Eng Comput*. 2008;46(8):745-757. doi:10.1007/s11517-008-0346-7

27. Reddy VY, Anter E, Rackauskas G, et al. Lattice-Tip Focal Ablation Catheter That Toggles between Radiofrequency and Pulsed Field Energy to Treat Atrial Fibrillation: A First-in-Human Trial. *Circ Arrhythmia Electrophysiol*. 2020;(June):483-495. doi:10.1161/CIRCEP.120.008718

28. Garcia-Sanchez T, Mercadal B, Polrot M, et al. Successful tumor Electrochemotherapy using Sine Waves. *IEEE Trans Biomed Eng*. 2019:1. doi:10.1109/TBME.2019.2928645

29. Merla C, Pakhomov AG, Semenov I, Vernier PT. Frequency spectrum of induced transmembrane potential and permeabilization efficacy of bipolar electric pulses. *Biochim Biophys Acta - Biomembr*. 2017;1859(7):1282-1290. doi:10.1016/j.bbamem.2017.04.014

30. Rogers WR, Merritt JH, Comeaux JA, et al. Strength-duration curve an electrically excitable tissue extended down to near 1 nanosecond. *IEEE Trans Plasma Sci*. 2004;32(4 II):1587-1599. doi:10.1109/TPS.2004.831758

31. Mercadal B, Arena CB, Davalos R V., Ivorra A. Avoiding nerve stimulation in irreversible electroporation: A numerical modeling study. *Phys Med Biol*. 2017;60(20):8060-8079. doi:10.1088/1361-6560/aa8c53

32. Wittkampf FHM, van Es R, Neven K. Electroporation and its Relevance for Cardiac Catheter Ablation. *JACC Clin Electrophysiol*. 2018;4(8):977-986. doi:10.1016/j.jacep.2018.06.005

33. Mir LM, Bureau MF, Gehl J, et al. High-efficiency gene transfer into skeletal muscle mediated by electric pulses. *Proc Natl Acad Sci U S A*. 1999;96(8):4262-4267.

34. Kranjc M, Miklavčič D. Electric Field Distribution and Electroporation Threshold. In: Miklavčič D, ed. *Handbook of Electroporation*. Cham: Springer International Publishing; 2017:1043-1058. doi:10.1007/978-3-319-32886-7_4

35. García-Sánchez T, Leray I, Ronchetti M, Cadossi R, Mir LM. Impact of the number of electric pulses on cell electrochemotherapy in vitro: Limits of linearity and saturation. *Bioelectrochemistry*. 2019;129:218-227. doi:10.1016/j.bioelechem.2019.05.021

36. Zhang Y, Lyu C, Liu Y, Lv Y, Chang TT, Rubinsky B. Molecular and histological study on the effects of non-thermal irreversible electroporation on the liver. *Biochem Biophys Res Commun*. 2018;500(3). doi:10.1016/j.bbrc.2018.04.132

37. Batista Napotnik T, Polajžer T, Miklavčič D. Cell death due to electroporation – A review. *Bioelectrochemistry*. 2021;141. doi:10.1016/j.bioelechem.2021.107871

38. Brock RM, Beitel-White N, Davalos R V., Allen IC. Starting a Fire Without Flame: The Induction of Cell Death and Inflammation in Electroporation-Based Tumor Ablation Strategies. *Front Oncol*. 2020;10(July):1-9. doi:10.3389/fonc.2020.01235

39. Beebe S, Sain N, Ren W. Induction of Cell Death Mechanisms and Apoptosis by Nanosecond Pulsed Electric Fields (nsPEFs). *Cells*. 2013;2(1):136-162. doi:10.3390/cells2010136

40. Mercadal B, Beitel-White N, Aycock KN, Castellví Q, Davalos R V., Ivorra A. Dynamics of Cell Death After Conventional IRE and H-FIRE Treatments. *Ann Biomed Eng*. 2020;48(5):1451-1462. doi:10.1007/s10439-020-02462-8

41. Kos B. Treatment planning for electrochemotherapy and irreversible electroporation of deep-seated tumors. In: *Handbook of Electroporation*. ; 2017. doi:10.1007/978-3-319-32886-7_2

42. Reddy VY, Neuzil P, Koruth JS, et al. Pulsed Field Ablation for Pulmonary Vein Isolation in Atrial Fibrillation. *J Am Coll Cardiol*. 2019;74:315-326. doi:10.1016/j.jacc.2019.04.021

43. Fusco R, Di Bernardo E, D'Alessio V, Salati S, Cadossi M. Reduction of muscle

contraction and pain in electroporation-based treatments: An overview. *World J Clin Oncol*. 2021;12(5):367-381. doi:10.5306/wjco.v12.i5.367

44. Yavin H, Shapira-Daniels A, Barkagan M, et al. Pulsed Field Ablation Using a Lattice Electrode for Focal Energy Delivery: Biophysical Characterization, Lesion Durability, and Safety Evaluation. *Circ Arrhythmia Electrophysiol*. 2020:529-538. doi:10.1161/CIRCEP.120.008580

45. Koruth J, Kuroki K, Iwasawa J, et al. Preclinical Evaluation of Pulsed Field Ablation: Electrophysiological and Histological Assessment of Thoracic Vein Isolation. *Circ Arrhythmia Electrophysiol*. 2019;12(12):1-9. doi:10.1161/CIRCEP.119.007781

46. Deodhar A, Dickfeld T, Single GW, et al. Irreversible electroporation near the heart: Ventricular arrhythmias can be prevented with ECG synchronization. *Am J Roentgenol*. 2011;196(3):330-335. doi:10.2214/AJR.10.4490

47. Reddy VY, Anic A, Koruth J, et al. Pulsed Field Ablation in Patients With Persistent Atrial Fibrillation. *J Am Coll Cardiol*. 2020;76(9):1068-1080. doi:10.1016/j.jacc.2020.07.007

48. Kaminska I, Kotulska M, Stecka A, et al. Electroporation-induced changes in normal immature rat myoblasts (H9C2). *Gen Physiol Biophys*. 2012;31(1):19-25. doi:10.4149/gpb_2012_003

49. Hunter DW, Kostecki G, Fish JM, Jensen JA, Tandri H. In Vitro Cell Selectivity of Reversible and Irreversible: Electroporation in Cardiac Tissue. *Circ Arrhythmia Electrophysiol*. 2021:440-448. doi:10.1161/CIRCEP.120.008817

50. Prado LNS, Goulart JT, Zoccoler M, Oliveira PX. Ventricular myocyte injury by high-intensity electric field: Effect of pulse duration. *Gen Physiol Biophys*. 2016;35(2). doi:10.4149/gpb_2015047

51. Dermol J, Miklavčič D. Mathematical Models Describing Chinese Hamster Ovary Cell Death Due to Electroporation In Vitro. *J Membr Biol*. 2015;248(5). doi:10.1007/s00232-015-9825-6

52. Perera-Bel E, Mercadal B, Garcia-Sanchez T, Gonzalez Ballester MA, Ivorra A. Modeling methods for treatment planning in overlapping electroporation treatments. *IEEE Trans Biomed Eng*. 2021. doi:10.1109/TBME.2021.3115029

53. Garcia PA, Rossmeisl JH, Neal RE, Ellis TL, Davalos R V. A parametric study delineating irreversible electroporation from thermal damage based on a minimally invasive intracranial procedure. *Biomed Eng Online*. 2011;10(1):34. doi:10.1186/1475-

925X-10-34

54. Andreuccetti D, Fossi R, Petrucci C. An Internet resource for the calculation of the dielectric properties of body tissues in the frequency range 10 Hz - 100 GHz. IFAC-CNR. [Online]. Available: http://niremf.ifac.cnr.it/tissprop/. Accessed on 2021-10-01.

55. Ivorra A, Al-Sakere B, Rubinsky B, M Mir L. Use of conductive gels for electric field homogenization increases the antitumor efficacy of electroporation therapies. *Phys Med Biol*. 2008;53(22):6605. http://stacks.iop.org/0031-9155/53/i=22/a=020.

56. Wittkampf FHM, van Es R, Neven K. Electroporation and its Relevance for Cardiac Catheter Ablation. *JACC Clin Electrophysiol*. 2018;4:977-986. doi:10.1016/j.jacep.2018.06.005

S.1 In vitro experiments

S.1.1 Methods

In vitro experiments were performed as a previous step to the in vivo experiments to obtain a first characterization and range of values of the dependence of IRE efficacy on the frequency of the biphasic waveform applied. Monophasic pulses were also used for comparison. Some other studies provided a wide range of lethal EF thresholds in cardiac and non-cardiac cells for different waveforms [48–50]

CHO cells were grown in complete cell culture medium which consisted of Dulbecco's Modified Eagle Medium (DMEM) with addition of 10% fetal bovine serum and supplemented by antibiotics (100 U/ml penicillin, and 100 μg/ml streptomycin). The cells were maintained in a humidified atmosphere at 37°C and 5% CO_2 and routinely passed every two days.

On the day of the experiment and after trypsinization, cells were centrifuged for 5 min and resuspended at a density of 1.2×10^6 cells/ml in a low conductivity buffer (LCB) to minimize electrolysis and thermal damage. LCB consisted of 250 mM Sucrose, 10 mM glucose, 10 mM NaCl, 5 mM KCl, 2 mM MgCl2, 10 mM HEPES, 1.8 mM CaCl2 (pH: 7.17, conductivity: 2.5 mS/cm, osmolarity: 305 mOsm). Cells suspended in LCB were exposed to electroporation EFs in conventional 1 mm cuvettes. After the delivery of the EF, cells were kept in the cuvettes for 10 min at room temperature. They were then sequentially diluted in complete medium and seeded in technical triplicates at 150 cells per cell culture well (of a 12-well culture plate) to measure their viability through a quantitative cloning efficacy test. After 5 days maintained in a humidified atmosphere, colonies were washed with PBS and fixed/stained with a crystal violet solution (0.2% Crystal Violet, 10% formaldehyde and 20% ethanol in H_2O). The number of clones N for each condition was counted. Viability was normalized to the number of clones in the control (Ncontrol) and reported as a percentage of survival: N/Ncontrol × 100. The cells in the controls were handled exactly the same way than the exposed cells including incubation times in cuvettes and dilutions. All the experiments were repeated at least three independent times in at least two different days.

The results of cell survival as a function of EF intensity were characterized with a mathematical probabilistic model[51]. In the present study we used a logistic regression as proposed in Perera et al. [52]. Probability of cell survival (Ps) was defined as:

$$P_s(\%) = 100\frac{1}{(1+e^{-(\beta_0+\beta_1 E))})}$$

where, β_0 provides information about the field magnitude at which the transition from living to dead cells occurs and β_1 describes its slope. Matlab 2020a (Mathworks) curve fitting toolbox was

used to fit the data. Finally, for each waveform studied, the EF threshold was derived as the intensity at which 95 % of cells were dead according to the fitted logistic regression.

S.1.2 In vitro cell survival experiments results

In Fig. S1a cell survival results obtained from cloning efficacy experiments and the corresponding fitted logistic regression models are shown for the different conditions studied. As expected, cell survival decreases when the intensity of the EF increases. Furthermore, the EF magnitude necessary to obtain equivalent survival rates considerably increases with frequency. In Fig. S1b the EF thresholds necessary to obtain a 95 % of cell death that were obtained from the logistic models are displayed for each frequency studied. Note that the data corresponding to monophasic pulses is displayed in the low frequency range because square pulses are considered as a quasi-DC waveform. Under these specific experimental conditions, the EF threshold value obtained for monophasic pulses is 1180 V/cm, for biphasic waveforms of 150 kHz is 1412 V/cm, for 250 kHz is 1616 V/cm and for 450 kHz 2024 V/cm. These results show how the EF intensity necessary to obtain an equivalent IRE effect depends non-linearly on the frequency of the waveform applied.

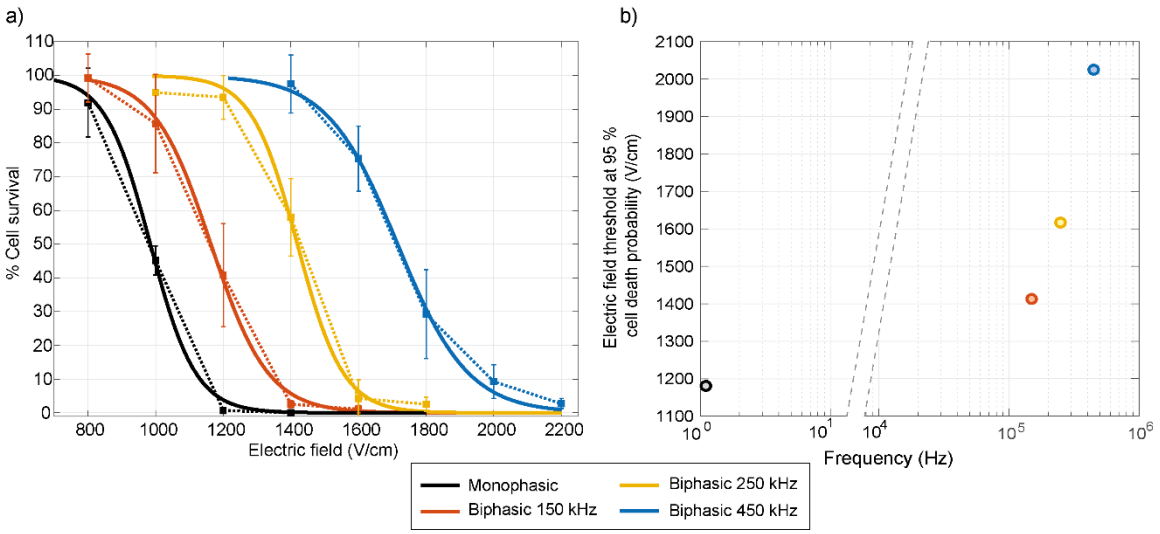

Fig. S1 Results from the in vitro study. a) Cell survival results from the cloning efficacy experiments as a function of EF intensity and the resulting fitted cell death probability models. b) EF magnitude necessary to obtain a 95 % of cell death as a function of the frequency of the applied waveform (values were extracted from the probabilistic models). Note that results from monophasic pulses are placed at very low quasi-DC frequency. For convenience, logarithmic scale of x-axis was broken to improve representation of data.

S.2 Computational model methods

The numerical model simultaneously solved the electric potential, the temperature and the electrical conductivity (σ) distributions in the treatment region during EF application using the coupled physics feature of COMSOL in a time dependent study. The heat source in the system corresponds to the Joule heating produced by the passage of an electric current through a conductor ($\vec{J} \cdot \vec{E}$), where $\vec{E}$ is the electric field and $\vec{J}$ is the current density ($\vec{J} = \sigma \vec{E}$). The conductivity dependence of ionic solutions on temperature variations was also modeled with a linear approximation. Additionally, to account for the EP phenomenon, the conductivity σ of the heart tissue was defined as a sigmoid function of the local EF magnitude, $|\vec{E}|$. Additionally, conductivity of heart tissue also included the contribution of temperature changes.

The conductivity model $\sigma(\vec{E}, T)$ used in the numerical simulations that included contributions of both electric field and temperature was[53]:

$$\sigma(\vec{E}, T) = \Delta_\sigma e^{-e^{-[b(|\vec{E}|-E_0)]}} + \sigma_0(1 + \alpha(T - T_0)) \quad (1)$$

where σ_0 is the initial conductivity of the non-electroporated tissue, Δ_σ is the maximum conductivity variation between a non-electroporated and fully-electroporated tissue, b represents the span of the transition zone, E_0 represents the electric field at which conductivity starts to increase due to the electroporation phenomenon, T_0 is the initial temperature (37 °C) and α=0.015 stands for the increase of 1.5 % in conductivity increase of ionic solutions per temperature degree.

The values used for σ_0 were extracted from the IFAC-CNR database[54] for each frequency (monophasic square pulses were approximated to the values at 10 Hz). For parameter b, the value was obtained from data in the literature corresponding to monophasic square pulses and muscle tissue[55] and was maintained constant for all conditions. As for E_0, there is no available data in the literature for myocardial tissue in vivo. In fact, most of the recent studies dealing with PFA refer to threshold values extracted from in vitro experiments[48] that are around 400 V/cm and that may substantially differ from the actual values required in vivo[32]. Based on that value, in the present simulations we arbitrarily assumed a value of E_0=500 V/cm for monophasic 100 µs pulses. E_0 values for the biphasic pulses at the different frequencies studied were scaled according to the behavior observed in the irreversible electric field threshold obtained in the vitro results presented in this study for CHO cells (refer to next section S2.2). Finally, the values of Δ_σ for monophasic pulses were the same values than those used in the literature for muscle tissue[55]. The values of Δ_σ for the biphasic pulses at the different frequencies studied were chosen to ensure that the conductivity value of the heart tissue at high electric field intensities (fully electroporated tissue) is similar for all cases.

The blood conductivity dependence on the electric field was not considered in the model because

there is no available data in the literature. Approximating blood behavior to other solid tissues would be highly speculative because only around 50% of blood volume is occupied by cells.

The complete list of values assigned to all parameters and the electrical and thermal properties used in the model can be found in Table TS1. The dependence of electric field intensity on conductivity of heart tissue is plotted for both monophasic pulses and biphasic bursts at the different frequencies simulated in Fig. S2.

Tissue/Material	Condition	Electrical			
		σ_0(S/m)	Δ_σ (S/m)	b (V/cm)$^{-1}$	E_0(V/cm)
Heart	Monophasic (DC)	$5.37\cdot 10^{-2}$	0.3	0.01	500
	Biphasic (90 kHz)	0.2119	0.14	0.01	600
	Biphasic (260 kHz)	0.2485	0.105	0.01	900
	Biphasic (450 kHz)	0.2747	0.08	0.01	1300
Blood	Monophasic (DC)	0.7	-	-	-
	Biphasic (90 kHz)	0.7	-	-	-
	Biphasic (260 kHz)	0.71	-	-	-
	Biphasic (450 kHz)	0.74	-	-	-
Electrodes	-	$4.03\cdot 10^{6}$	-	-	-

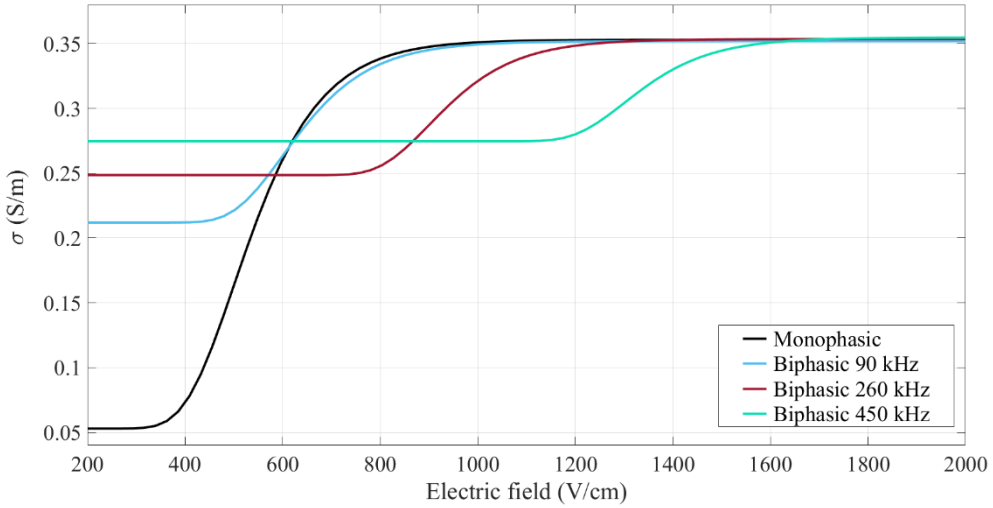

Fig. S2 Modelled conductivity dependence of the heart tissue with the electric field intensity $\sigma(\vec{E})$ for the different waveforms studied.

	Thermal		
	$\rho(kg/m^3)$	k(W/(m$\cdot K$))	$C_p(J/(kg\cdot K))$
Heart	1081	0.56	3686
Blood	1060	0.5	3840
Electrodes	7850	44.5	475

Table TS1 Summary of electrical conductivity and thermal properties used in the computational model for the different tissues/materials. Fig. S2 depicts the conductivity dependence with electric field for the heart tissue at the different frequencies studied.

S.3 Thermal simulations

The computational model was also used to estimate the risk of thermal damage of the experimental electric field delivery protocols. Similar to radiofrequency ablation, the heating source in the present study is due to Joule heating produced by the passage of an electric current through a conductor ($\vec{J} \cdot \vec{E}$). As previously explained conductivity of cardiac tissue was modeled with a double dependence with electric field and temperature $\sigma(\vec{E}, T)$. The numerical model simultaneously solved the electric potential, the temperature and the electrical conductivity distributions in the treatment region during pulse application using the coupled physics feature of COMSOL in a time dependent study. Subsequently, only the temperature dynamics was solved in the period between pulses (1 second). This two-step process was sequentially repeated 10 times (the number of pulses/bursts applied), updating in each step the initial values from the previous iteration. Only heat conduction using the heat transfer in solids equations was modelled. An initial temperature for the tissue and the electrode of 32 ºC (corresponding to the temperature measured by the sensor) was considered, the rest of boundaries were fixed at 20 ºC.

In Fig. S3 an example of the results obtained from simulations at a biphasic frequency of 90 kHz and the two voltage levels applied (500 and 800) is shown. The temperature evolution is shown at the point of contact between the electrode and the tissue, reproducing the position of the optical temperature probe used in the experiments. As in the real in vivo recordings, the temperature sharply increases during each EP burst (Joule heating) and subsequently slowly dissipates by conduction between consecutive bursts. The maximum absolute temperature variations provided

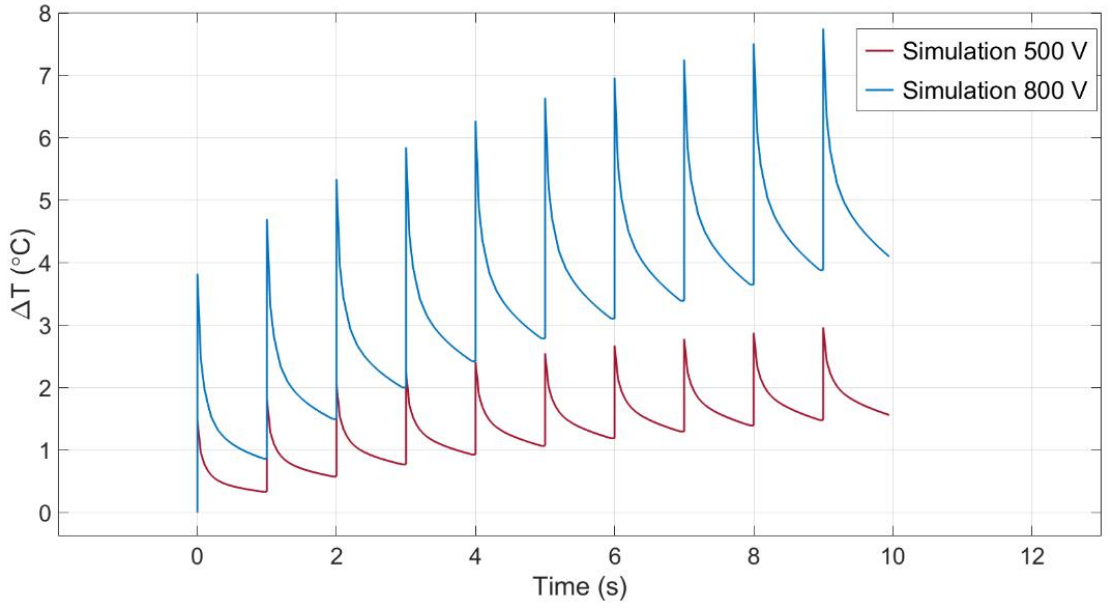

Fig. S3 Results from thermal simulations obtained with a biphasic frequency of 90 kHz and the two voltage levels applied (500 and 800). The temperature variation evolution is shown at the point of contact between the electrode and the tissue for a complete 10-burst sequence.

by the model are significantly higher than the actual measurements performed in vivo (roughly around 3 times higher) but still provide values away from thermal damage.

The deviation between the real measurements and the simulations can be explained by the simplifications assumed in the model. Specially, the heat dissipation effects that the metallic electrode has in the tissue are likely underestimated. Also, actual material properties could differ from the values used in the model (the thermal material properties used are nor specific for ventricular epicardium neither specific for the animal model used in the study). More sophisticated modelling strategies could be implemented if the goal was to obtain the most realistic results. However, as the goal of these simulations was to evaluate the risk of thermal damage in a worst case scenario, overestimating the possible heating provides a safety margin that ensures no thermal damage.

S.4 Representative ECG traces

Examples of ECG traces for all conditions are provided in Fig. S4 demonstrating that no significant changes were produced either immediately after or at 3 weeks after treatment. All traces correspond to recordings performed with the chest of the animals closed. Any of the PFA protocols induced ventricular nor supraventricular arrhythmias.

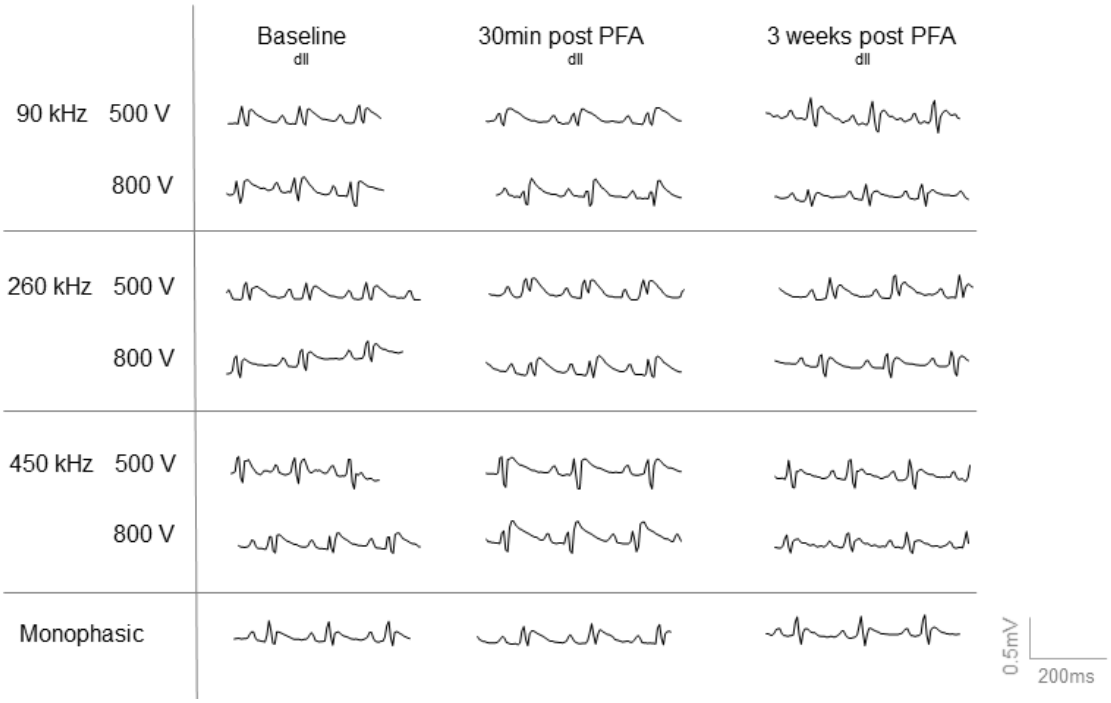

Fig. S4 Representative examples of ECG traces on derivation dII at baseline, 30 min after PFA treatment (thorax already closed) and 3 weeks after PFA treatments.

S.5 Histopathological observations

Observation of the trichrome-stained histological sections by an expert pathologist confirmed fibrosis in the blue-stained areas with preserved structure in arterioles, venules and the rest of medium diameter vessels (see high magnification examples in **¡Error! No se encuentra el origen de la referencia.** lower panels). Lesions displayed homogeneous fibrosis with no evidence of tissue sparing around blood vessels (no effect of blood flow cooling). Signs of perivascular chronic inflammation were observed in some instances at the subepicardial level. In some lesions small surviving cardiomyocytes cores were observed. Most lesions presented relatively well-defined borders with some areas of jagged borders and fibrotic infiltration.

Video legends

Supplementary Video 1. Example of video recording of a complete PFA application corresponding to monophasic pulses at 500 V showing the level of contractions induced.

Supplementary Video 2. Example of video recording of a complete PFA application corresponding to a biphasic waveform of 90 kHz at 500 V showing the level of contractions induced.

Supplementary Video 3. Example of video recording of a complete PFA application corresponding to a biphasic waveform of 260 kHz at 500 V showing the level of contractions induced.

Supplementary Video 4. Example of video recording of a complete PFA application corresponding to a biphasic waveform of 450 kHz at 500 V showing the level of contractions induced.